Biomaterials Science

ROYAL SOCIETY OF CHEMISTRY

PAPER

View Article Online
View Journal | View Issue

Cite this: *Biomater. Sci.*, 2025, **13**, 4706

4D-printed multifunctional hydrogels as flexible strain sensors and nerve conduits†

Akshat Joshi,‡[a] Saswat Choudhury, ‡[a] Arabinda Majhi,[b] Sampath Parasuram,[c] Vageesh Singh Baghel,[d] Samrat Chauhan,[e] Supriya Khanra,[e] Debrupa Lahiri[b] and Kaushik Chatterjee *[a,c]

Conductive hydrogels are critical for advanced bioelectronics and the repair of electroactive tissues. However, developing conductive hydrogels into complex biomimetic shapes with good flexibility and bioactivity poses a major biofabrication challenge. This study utilizes dual-component hydrogel inks based on alginate incorporating conductive fCNT (acid-functionalized carbon nanotube) nanofillers, with the composite gel exhibiting an electrical conductivity of 6.6 ± 0.5 mS cm^{-1} at 2 mg ml^{-1} fCNT loading. Owing to their good combination of electrical conductivity and mechanical properties, the (three-dimensional) 3D-printed gels were successfully applied as strain sensors to sense subtle human motions, such as finger and elbow bending. Bilayered hydrogels prepared through four-dimensional (4D) printing exhibited programmable shape changes owing to differential swelling post-printing to yield nerve guidance conduits (NGCs) of intricate and tissue-adaptable designs, such as single and multichannel and bifurcated designs, based on accurate prediction by finite element analysis. The proliferation of neural cells was enhanced on the fCNT-gel compared to the neat gel. Sutureless deployment and enhanced peripheral nerve regeneration were established for the fCNT-gel in a rat sciatic nerve injury model. Overall, this work presents the fabrication of 4D-printed multifunctional conductive hydrogels, which can find diverse applications ranging from implantable nerve conduits to strain sensing.

Received 3rd February 2025,
Accepted 9th July 2025

DOI: 10.1039/d5bm00166h

rsc.li/biomaterials-science

1. Introduction

Bioelectronics has emerged as a new field of research, replacing traditional rigid devices with soft, flexible, and miniaturized components.[1] Future bioelectronic devices warrant the use of conductive hydrogels with superior flexibility, softness, and biocompatibility. Multifunctional conductive hydrogels have been extensively used in diverse fields, such as biosensors,[2] tissue engineering,[3] flexible electronics,[4] human–machine interaction,[5] health monitoring,[6] *etc*. However, most conductive gels are limited by their processability by conventional techniques, such as molding,[7] blending,[8] thermal polymerization,[9] copolymerization,[10] electrospinning,[11] *etc*. There are only a few reports on the successful fabrication of conductive gels *via* additive manufacturing techniques into complex biomimetic shapes. Other limitations include the compromise between conductivity and mechanical compliance, increased viscosities due to higher amounts of conductive nanofillers, and poor tissue adaptability.[12] Conductive gels have previously been prepared by either using conducting polymers, such as polypyrrole,[13] polyaniline,[14] and PEDOT[15] (poly(3,4-ethylene dioxythiophene)) or by incorporating conductive fillers, such as gold nanoparticles,[16] CNTs (carbon nanotubes),[17] graphene,[18] *etc*., into polymeric matrices. However, there are significant challenges that preclude their use in the final application. Conducting polymers exhibit wide variations in conductivity with minor changes in their structures, and the carbon-based nanofillers are prone to poor dispersion and, hence, limited processability.

Conductive gels find use as flexible strain sensors to sense subtle human motions[19] and in the repair of electroactive tissues, such as neural,[20] cardiac,[21] and skeletal muscles.[22] In recent times, neural tissue engineering has witnessed a paradigm shift towards gel-based nerve guidance conduits (NGCs).[23] An ideal NGC should exhibit permeability, mechanical flexibility, a

[a]*Department of Bioengineering, Indian Institute of Science, C.V. Raman Avenue, Bangalore 560012, India. E-mail: kchatterje@iisc.ac.in; Tel: +91-80-22933408*
[b]*Biomaterials and Multiscale Mechanics Lab, Department of Metallurgical and Materials Engineering, Indian Institute of Technology Roorkee, Roorkee 247667, India*
[c]*Department of Materials Engineering, Indian Institute of Science, C.V. Raman Avenue, Bangalore 560012, India*
[d]*Department of Mechanical Engineering, Indian Institute of Science, C.V. Raman Avenue, Bangalore 560012, India*
[e]*Chitkara College of Pharmacy, Chitkara University, Punjab 140401, India*
†Electronic supplementary information (ESI) available. See DOI: https://doi.org/10.1039/d5bm00166h
‡Equal contribution.

suitable degradation profile, tissue adaptability, and electrical conductivity for improved peripheral nerve repair.[24] Soft hydrogels have been recognized as multifunctional NGCs, as they meet most of these requirements. However, even hydrogel-based NGCs suffer from several drawbacks, including a lack of suturability, limited designs to accommodate complex nerve defects, and the absence of inherent biochemical or electrical cues that can accelerate nerve regeneration.[25] The electroactive properties of NGCs are crucial for the successful restoration of severed nerves, as they allow electricity transmission and activation of critical intracellular signaling pathways in electroactive neural tissues.[26] Considering the previous advantages of gel-based NGCs, conductive gels with biomimetic shapes could offer a viable solution for treating peripheral nerve injury due to the synergistic effect of electrical cues and the ability of gels to mimic the native neural tissue.

To date, most conductive gel-based NGCs have been prepared by traditional methods, such as molding,[27] dip-coating,[28] and electrospinning.[29] These hinder the possibility of complex designs of NGCs and customization suiting the individual needs of different patients. Advancements in additive manufacturing techniques, including four-dimensional (4D) printing, have led to the development of more dynamic, intricate, and tissue-adaptable medical devices.[30] 4D printing involves the use of stimuli-responsive materials, such as shape memory polymers, composites,[31] multi-component hydrogels,[32] *etc.*, often combined with anisotropic design principles[33] to realize programmable shape changes post-printing. The shape changes are a consequence of the interaction of stimuli with the 3D-printed part.[34] However, 4D fabrication has been rarely explored to prepare conductive hydrogel-based multifunctional NGCs.[35] One study utilized a shape memory polymer incorporated with conductive MXene nanosheets to prepare temperature-activated self-rolled NGCs;[36] however, the fabrication involves organic solvents and warrants multiple post-printing steps, such as freeze-drying and wrapping around a glass rod, and the stimulation relies solely on body temperature, which makes it unreliable and limits translation. We had earlier reported dual-component gels prepared by extrusion-based 3D printing that could self-roll *in situ* due to swelling gradients, forming hollow NGCs to clamp the distal and proximal ends of the severed nerve, thereby guiding the axons without the need for sutures.[37] However, no studies have integrated electrical cues and complex tissue-adaptable designs to imitate the neural architecture with the sutureless neurorrhaphy technique. Such a synergistic technology will make the surgical procedure easier and patient-compliant and effectively enhance the functional recovery of neurons.

In the current study, multifunctional dual-component conductive hydrogels were utilized to develop bioinks with adequate printability through extrusion-based printing. The configured bioink (composition was carefully chosen to create significant swelling differences across the layers) was printed using optimized parameters. Given its good mechanical properties and electrical conductivity, the fCNT-gel was employed as a strain sensor to detect subtle human motions, such as elbow and finger bending. Coupled with predictive FEA simulations, several structures were printed that can yield different biomimetic designs of NGCs, such as single-channel, multichannel, and bifurcated hollow tubes post-printing (Fig. 1). Owing to the high electrical conductivity of the gels, the NGCs with fCNT revealed improved neural regeneration compared to the pristine gel NGCs. Overall, the technique proposed in the current research can open new avenues for diverse applications, including next-generation NGCs with improved peripheral nerve regeneration and strain sensors.

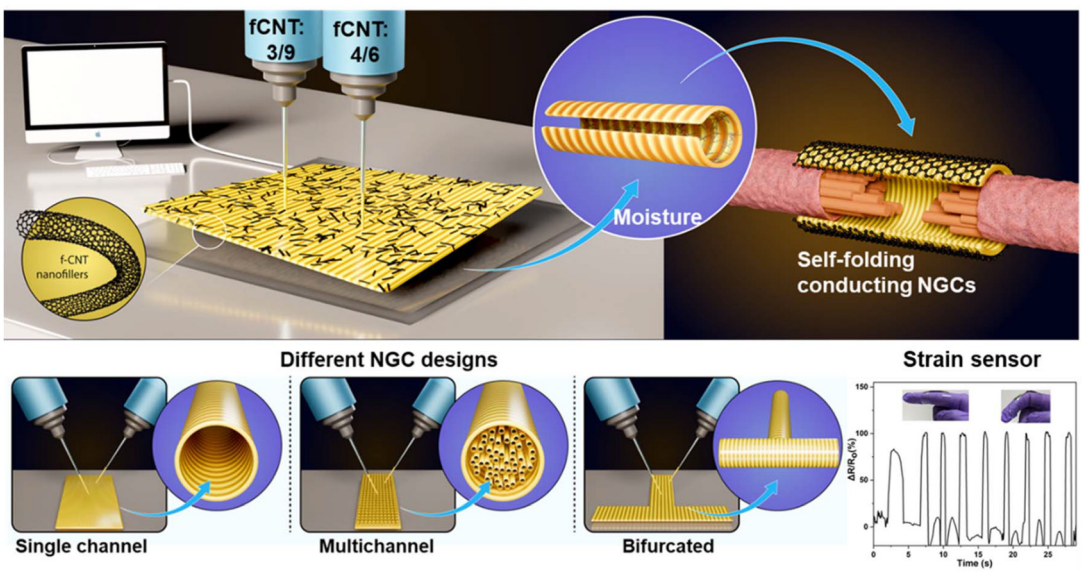

Fig. 1 Schematic demonstration of 3D printing of conductive hydrogel inks at two different concentrations and application in strain sensing and different designs of self-folding NGCs.

2. Results and discussion

Carbon nanotubes (CNTs) are known to have excellent electrical conductivity owing to their electronic structure.[38] However, they tend to agglomerate, forming bundles due to strong van der Waals interactions and minimal affinity towards non-carbonaceous materials. Acid functionalization of CNTs is a popular technique to overcome this issue of poor dispersion in polymeric matrices, especially in polar solvents, such as water.[39] In this work, CNTs were functionalized with carboxyl end groups *via* acidic treatment in the liquid phase (Fig. S1a†). SEM micrographs indicate the fragmentation of CNTs upon chemical oxidation to form carboxylic acid-functionalized CNTs (referred to as fCNTs) (Fig. S1b–d†). fCNTs also exhibited higher oxygen content than the pristine CNTs in the EDX (energy dispersive X-ray) analysis (Fig. S1(e and f)†). fCNTs were used as nanofillers (2 mg mL^{-1}) in the hydrogels prepared from alginate and methylcellulose. The fCNT loading was optimized based on the electrical conductivity values and processability. 2 mg mL^{-1} fCNT loading exhibited lower impedance than 1 mg mL^{-1} (Fig. S2†), and any loading higher than 2 mg mL^{-1} led to frequent nozzle clogging during printing. Two different gel compositions (3% alginate with 9% methyl cellulose, *i.e.*, 3/9 and 4% alginate with 6% methyl cellulose, *i.e.*, 4/6) were selected based on the optimization in our previous study[37] to result in significant swelling differences. The gels incorporating fCNTs (referred to as fCNT-gel) were characterized to assess their rheological properties. Viscosity flow tests indicate the highly shear-thinning behavior of both composite gels, rendering them highly printable through extrusion-based 3D printing (Fig. 2Aa). The viscoelastic properties of the gels demonstrate that the storage moduli are higher than the loss moduli in the linear viscoelastic region (LVR) (Fig. 2Ab). Thixotropy tests of the gels of both compositions indicate their viscosity recovery behavior in response to shear stress. It can be seen that the viscosity of the gels drops under the application of high shear forces and consequently recovers to the original values upon withdrawal of the shear (Fig. 2Ac). This is due to the polymeric chain disentanglements and re-entanglements upon shear application and withdrawal, respectively. Hence, the rheological properties of the composite gels endow them with high printing accuracy and post-printing stability. Morphological characterization of the gels through SEM revealed larger pore sizes in the case of the fCNT-gel of 3/9 composition than that of 4/6 (Fig. 2Ad). This leads to considerable differences in the extent of swelling, with 3/9 exhibiting much higher % swelling (≈2 times) than 4/6 (Fig. S3†). The electrical conductivity of the fCNT-gels (6.6 ± 0.5 mS cm^{-1}) was significantly higher than their neat counterparts (3.1 ± 0.4 mS cm^{-1}) (Fig. 2Af) owing to the highly conductive fCNT fillers within the hydrogel matrix. Additionally, the impedance values of neat gels are higher in the entire tested frequency range (10–10^5 Hz), whereas the fCNT-gels exhibited much lower values (Fig. 2Ae).

Next, the mechanical properties of the fCNT-gels were determined to validate their suitability as strain sensors. The fCNT-gels demonstrated an elastic modulus of ≈0.65 MPa and were stretchable, with a strain of ≈15% before failing (Fig. 2Ba). Cyclic stress–strain plots indicate the robust fatigue performance of the gels, with the final strain at the end of every cycle close to that of the preceding cycle for up to four consecutive cycles of loading and unloading without failure (Fig. 2Bb). Furthermore, the shape recovery ability of the composite gels was assessed at a stress of 0.02 MPa. There is no prominent hysteresis, and the strain at the end of every cycle was maintained at ≈5.5%. The % strain recovery was ≈100% for up to twenty cycles (Fig. 1B(c and d)). The improved cyclic mechanical properties can be attributed to the good dispersion and reinforcing effect of the fCNT nanofillers in the gel. There was no apparent deformation and stress reduction with increasing strain for up to four loading–unloading cycles. This is indicative of a robust interaction between the fCNTs and polymeric chains of the hydrogel, aided by well-dispersed fCNTs in the gel. The excellent electrical conductivity of the fCNT-gel combined with its good mechanical properties offers the opportunity to convert external stimuli, such as strain or pressure, into detectable electrical signals.[40] To determine the efficacy of the conductive gels as strain sensors, $\Delta R/R_0$ was measured as a function of time and strain (Fig. 2B(e and f)). As seen from the calibration curve, $\Delta R/R_0$ increased monotonically with applied strain (till the strain at failure ≈15%), implying the applicability of the fCNT-gel as a strain sensor in the specified range. As a demonstration of monitoring human motions, the gel was placed on the finger and elbow, and the resulting $\Delta R/R_0$ was recorded in real time upon suitable movement of the finger and elbow. In the case of elbow flexing, a stable and repetitive pattern of resistance change was observed with the periodic movement of the elbow (Fig. 2Bg). Similarly, for finger bending, $\Delta R/R_0$ followed a stable trend with minimal fluctuations as the finger was bent and unbent periodically (Fig. 2Bh). The output $\Delta R/R_0$ signals remained stable and repeatable with minor fluctuations, which can be attributed to water evaporation. When the finger was bent with a stepwise increase in angles from 0 to 60°, 90°, and 150°, $\Delta R/R_0$ was 86, 94, and 99%, respectively (Fig. 2Bi). This indicates that the gel can sense different strain amplitudes.[41] Additionally, $\Delta R/R_0$ remained constant when the finger was held stable at a specific angle. These results demonstrate the effectiveness of the fCNT-gel as a potential strain sensor to detect subtle human motions with sufficient stability and repeatability.

Next, the fCNT-gels of two distinct compositions (3/9 and 4/6) were 3D-printed into flat sheets of suitable dimensions, air-dried completely, and then exposed to barium chloride solution. The flat sheets could then self-morph into complete hollow tubes due to the significant differences in the extent of water uptake between the two gel layers (Fig. 3A(a–d) and S3†). A computational model was devised to predict the shape deformations of the 4D-printed structures with encoded infill patterns. A thermal expansion model was employed to simulate the deformations of the hydrogels after establishing a quantitative correlation between the swelling model. The details of the model used are provided in the ESI (section 1.4, ESI†).

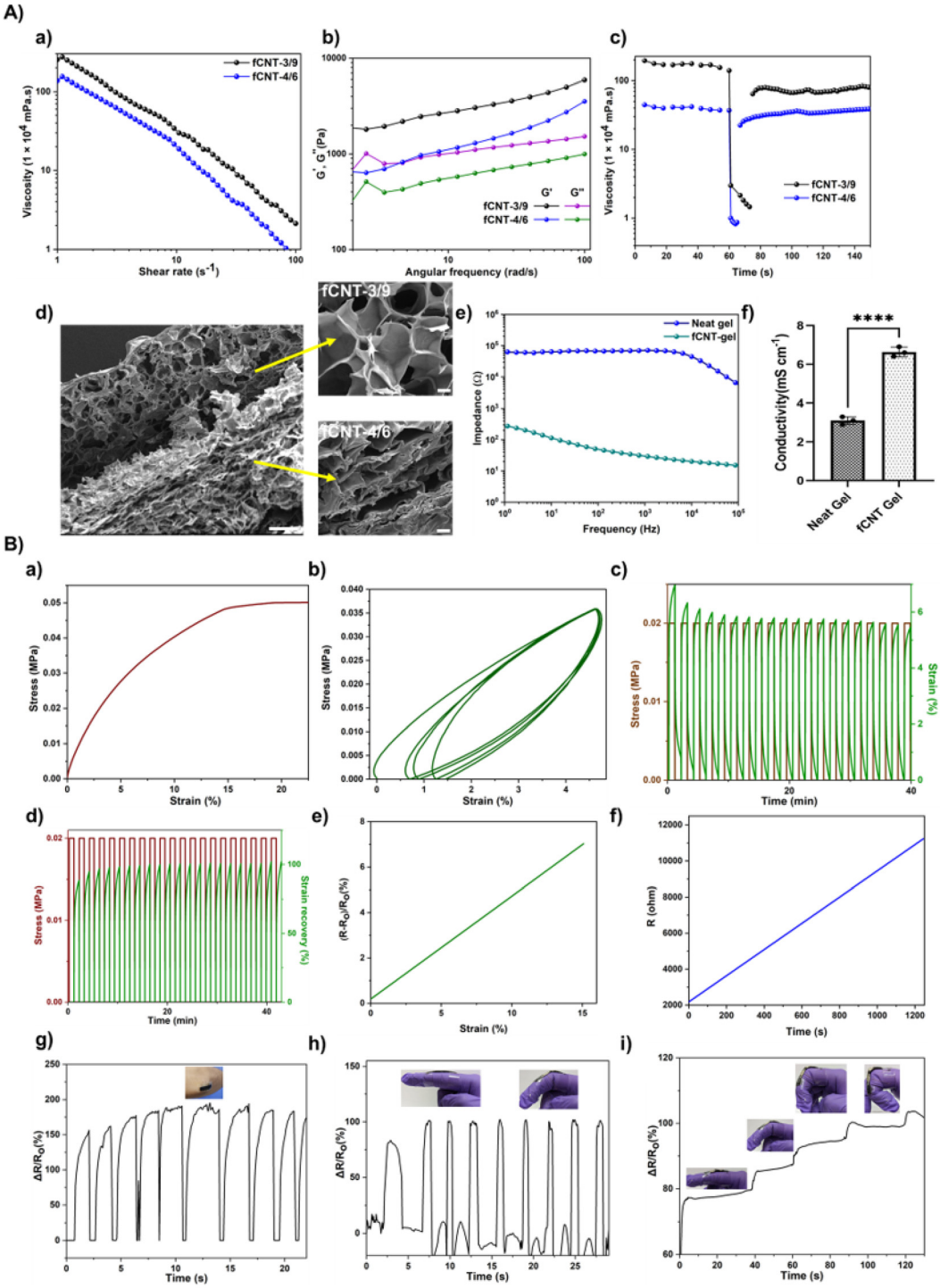

Fig. 2 Physico-chemical characterization of fCNT-gels. (A) (a) Viscosity flow test, (b) viscoelastic properties, (c) thixotropy assessment of fCNT-gels with 3 : 9 and 4 : 6 compositions; (d) cross-sectional SEM micrograph of the dual-component gel (scale: 500 μm) and the individual components (scale: 50 μm); (e) impedance *versus* frequency plot; (f) electrical conductivity of neat and fCNT-gels. (B) (a) Stress–strain plot, (b) cyclic stress–strain plot, (c) % strain and (d) % strain recovery of fCNT-gels; (e) calibration plot of fCNT-gel as a strain sensor; (f) resistance *versus* time profile of fCNT-gel; (g–i) fCNT-gels employed as strain sensors for detecting subtle human motions, such as (g) elbow bending, (h) finger bending, and (i) different stages of finger bending.

With the aim of obtaining a bifurcated NGC, an initial design of a T-shaped sheet was used, which later morphed into a perfusable, stable, and non-leaky T-junction (Fig. 3A(f–i) and Videos V1 and V2†). Bifurcated or T-junction NGC designs are posited to facilitate the separation of the growing axon bundles in a relatively biomimetic manner compared to

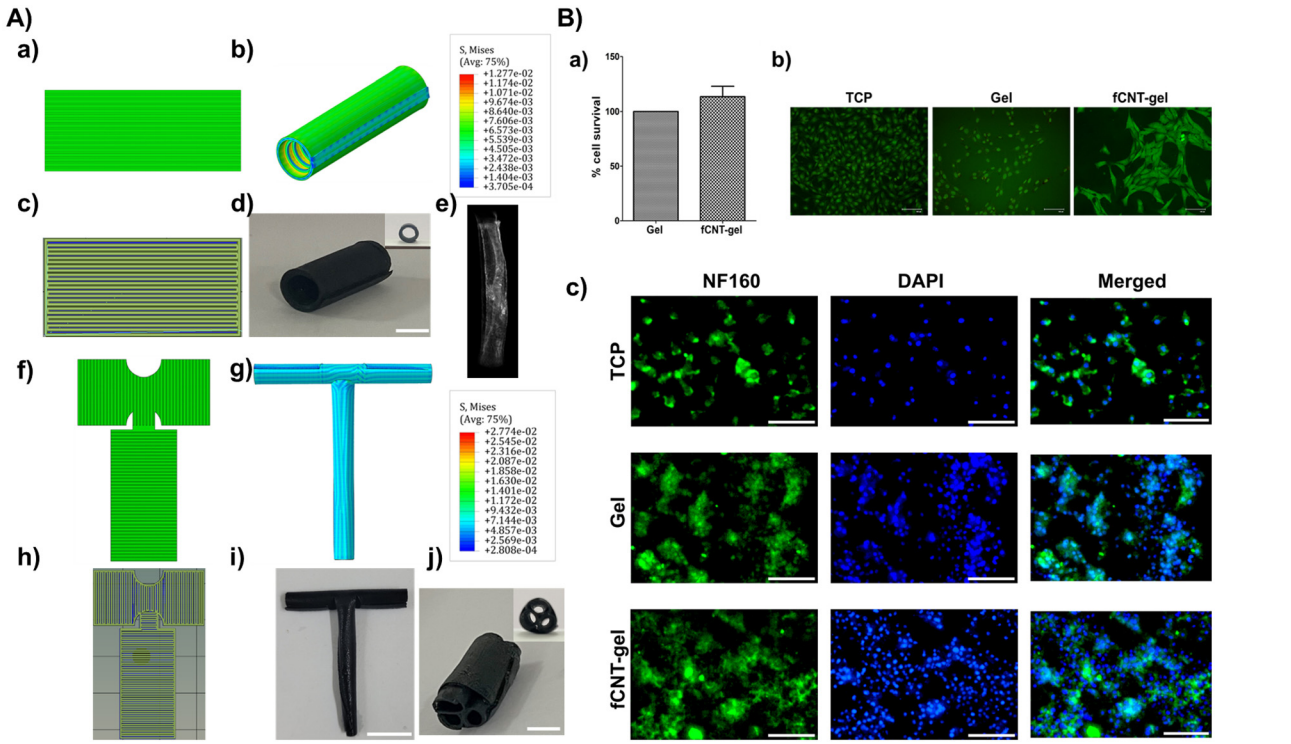

Fig. 3 4D printing and *in vitro* cell studies on the fCNT-gels. (A) Programmable and predictable shape changes in fCNT-gels to realize different designs of NGCs. (a and b) FEA simulation of a flat sheet (a) self-rolling into a hollow tube (b); (c and d) experimental demonstration of 3D-printed flat sheets of fCNT-gel of different compositions into hollow tubes driven by differential swelling (scale: 4 mm); (e) micro-CT imaging of the fCNT-gel NGC; (f and g) FEA simulation of a flat T structure transforming into a bifurcated T-junction; (h and i) experimental demonstration of a 3D-printed flat T-like structure folding into a bifurcated and perfusable NGC (scale: 10 mm); (j) fabrication of a multichannel NGC (scale: 4 mm). (B) *In vitro* cell culture on neat and fCNT-gels. (a) Alamar Blue assay of HT-22 cells cultured on 3D-printed fCNT-gels; (b and c) live–dead staining (b) and NF160 (green)-DAPI (blue) staining (c) of cells seeded on fCNT-gels on day 3 post-seeding (TCP: tissue culture plate; scale: 100 μm).

simple hollow tubes.[42] Similarly, multichannel NGCs were prepared by placing the self-rolled tubes of smaller diameters over a design-encoded flat sheet with a width similar to the lengths of the tubes, following which the sheet self-rolled into a hollow tube with the smaller tubes within its lumen (Fig. 3A(j) and Video V3†). Multichannel NGCs have been proven to effectively regenerate nerves by promoting the increased internal surface area for increased cell attachment,[43] limiting the dispersion of axons,[44] and offering higher mechanical stability and neuronal fascicular microstructure mimicking native nerves.[45] To endow these NGCs with non-invasive imaging capabilities, barium chloride was used to crosslink the printed fCNT-gels. The barium ion crosslinked fCNT-gels display good contrast in X-ray imaging owing to the inherent radiopacity of barium ions[46] (Fig. 3A(e)).

The *in vitro* cytocompatibility of neat and fCNT-gels was assessed using HT-22 (mouse hippocampal neuronal) cells. As seen from the Alamar Blue assay and live–dead staining, cellular viability was enhanced on fCNT-gels compared to neat gels owing to the presence of CNTs that are known to augment neuronal cell proliferation (Fig. 3B(a and b)). NF160 and nuclear staining revealed healthy morphology of cells in both neat and fCNT-gels, with more elongated cells observed on the fCNT-gels (Fig. 3Bc and Fig. S4†). This observation results from the favorable role of CNTs in promoting neurite extension.[47] Neurite outgrowth, or extension, is crucial for neuronal migration, differentiation, and synaptic plasticity. Facilitating neurite outgrowth is essential for enhancing nerve regeneration and attaining functional recovery in instances of neurological impairment or disease. It is well reported that carbonaceous nanomaterials facilitate direct electronic current flow, which leads to the redistribution of charge along the cell membrane surface and direct electrical coupling between neuronal cells.[48] Additionally, CNTs are also known to modulate downstream signaling by stimulating nerve growth factors and hence contribute to neurite outgrowth.[49]

The potential of neural regeneration of 4D-printed fCNT-gel conduits was estimated *in vivo* in a well-established 5 mm sciatic nerve defect in rats and monitored for up to 2 months and compared with neat polymeric (mentioned as gel) conduits (Fig. 4(A and B)). Both the gel and fCNT-gel conduits were able to intraoperatively self-wrap, thereby clamping the severed ends of the nerves upon exposure to barium chloride (Fig. S5†). The animals were randomly segregated into four groups: sham (no surgical damage), negative (no conduit at the injury site), neat (referred to as gel), and fCNT-gel. All experiments were carried out at the Chitkara College of Pharmacy, Chitkara University, India (approval number IAEC/

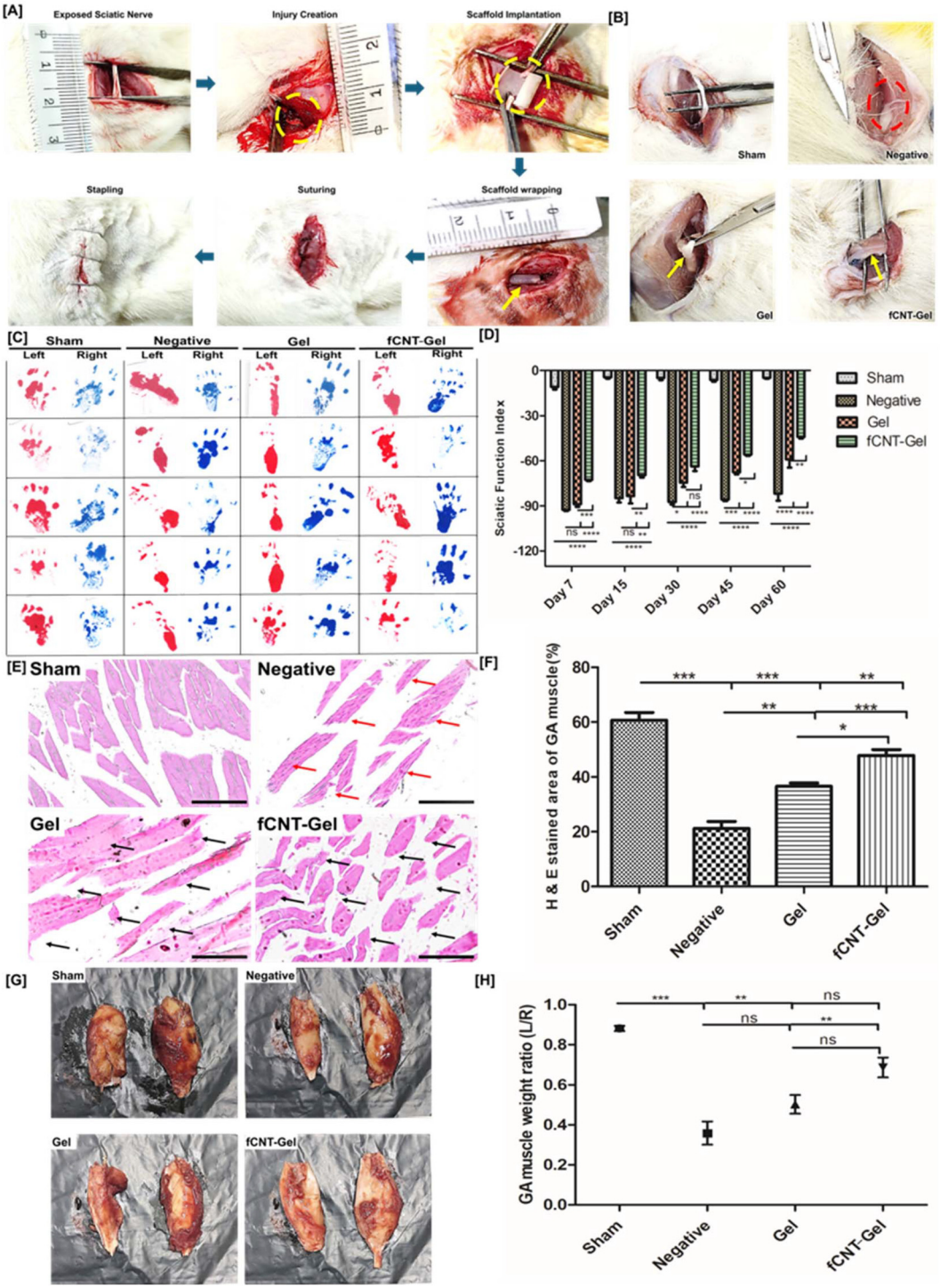

Fig. 4 *In vivo* assessment of neural regeneration in neat and fCNT-gels. (A) Demonstration of the sciatic nerve defect creation in the rat model; (B) digital images of the four groups (yellow arrow indicates the area of wrapped gels; red dotted circle indicates the non-regenerated area in the negative control); (C) digital images of the footprints of the left and right hind feet. Individual photos of left and right paw prints of animals from different groups at each time point were assembled to create the image. Red-colored paw print: left hind leg; blue-colored paw print: right hind leg; (D) quantitative estimation of SFI of different groups at each time point (*** denotes $p < 0.001$ and ns denotes non-significant); (E) H&E-stained images of the GA muscle of the left hind leg (operated limb) of rats from different experimental and sham groups (the degenerated muscle fibrils (in the negative group) and the regenerated muscle fibrils (gel and fCNT-gel groups) have been indicated with red and black arrows, respectively); (F) quantification of the H&E-stained area of the GA muscle. Data are presented as mean ± SD (n = 4); (G) digital images of the gastrocnemius muscle (GA) of different groups; (H) measurements of the GA wet weight ratio (left/right).

CCP/23/02/PR-16) and followed CCSEA (Committee for Control and Supervision of Experiments on Animals) guidelines. A combination of functional and structural assessments was used to quantitatively assess the nerve regeneration. Functional assessment, such as the sciatic function index (SFI), was performed at specific intervals for 2 months, after which rats were sacrificed to assess the restoration of motor function in the wound-inflicted leg.

SFI is a measure of the activity in the sciatic nerve. SFI was calculated by comparing the geometric representation of the damaged hind paw of an injured rat with the representation of the contralateral paw. Herein, the paw prints of the operated legs and their corresponding contralateral paws of the animals from all the groups were taken on the 7^{th}, 15^{th}, 30^{th}, 45^{th}, and 60^{th} days (compiled in Fig. 4C). In contrast to the negative control group, both the NGC-treated groups exhibited significant increments in SFI measurements on all the days post-surgery (Fig. 4D). The best SFI values for both the treated groups were observed on Day 60. However, between the two groups, the fCNT-gel group consistently exhibited a marked increase in SFI, demonstrating the superiority of conductive fCNT nanofillers in the gels compared to their neat counterpart.

Atrophy of the gastrocnemius muscle (GA) is a common complication following sciatic nerve damage. The regeneration of the sciatic nerve and reinnervation of the GA reduce muscle atrophy. GA weight analysis was used to evaluate muscle atrophy and neural regeneration. Post-sacrifice of the animals, the gastrocnemius muscles of both hind legs were removed and weighed. The left (L) (muscle weight of operated left leg)/right (R) (muscle weight of normal right leg) ratio was determined for all the groups (Fig. 4(G and H)). The lowest L/R ratio was observed for the negative group, whereas it was substantially improved in the case of conduit-treated groups. No significant difference in the L/R ratio was observed between the two treated groups (Fig. 4H). This observation was corroborated by the digital photographs of the gastrocnemius muscles (Fig. 4G). Muscle atrophy and regeneration were further assessed by hematoxylin and eosin (H&E) staining of the GA muscle (Fig. 4E), which revealed that the mass, integrity, and morphology of the muscle were considerably lost in the negative group. These parameters were markedly improved in animals treated with the 4D-printed NGCs (Fig. 4F), which were comparable to the sham group. Thus, both NGCs (gel and fCNT-gel) were successful in restoring the sciatic nerve, thereby reinnervating the gastrocnemius muscle and reducing muscular atrophy as a consequence of regeneration.

Histological investigation of the nerves in different groups revealed the success of neural tissue regeneration in the fCNT-gel groups. Regenerated nerve tissue was observed in the longitudinal slices of samples stained with H&E 2 months post-surgery (Fig. 5A). Here, the staining of the negative control group is excluded, as no nerve connection was established between the two resected ends. H&E staining of the cross sections (Fig. 5A[i–iii]) and longitudinal sections (Fig. 5A[iv–vi]) in the middle of the region covered by the gel-based NGC indicates the development of nerves and Schwann cells (SCs) into the implanted conduit, highlighting the restoration of injured nerves at the proximal end. Quantification of the H&E-stained positive area of the nerve from the gel and fCNT-gel groups (Fig. 5C) confirmed a higher amount of regenerating nerve fibers in the fCNT-gel group than in the former. Additionally, the integrity and morphology of the regenerated nerve were superior in the fCNT-gel group compared to the gel (Fig. 5(A and B)). This enhancement in the fCNT-gel group was possibly due to the conductive fCNT fillers in the lumen of the formed tube, which promote axon sprouting and nerve restoration. The electrical conductivity of the fCNT-gel provided an ideal environment for Schwann cells to grow on the fibers to utilize them as tracks on which the axon could be regenerated. The findings of the H&E staining demonstrated that the sham-operated group had intact nerve fibers. Nevertheless, further research is warranted to elucidate the underlying mechanisms.

Injury to peripheral nerves initiates a complex cascade of molecular events, eventually leading to nerve regeneration. These events include Wallerian degeneration, the axonal response for phagocytosis, chromatolysis, Schwann cell proliferation, axonal growth, and target reinnervation. NF160 (Neurofilament 160), a marker for neurofilaments, is typically seen in cells or tissues of neuronal origin. S100β (S100 calcium-binding protein B) is a characteristic marker for SCs. Thus, both the cross-sections and the longitudinal sections of the tissues were immunostained for NF-160 (green) and S100β (red), and the nuclei were counterstained with DAPI (Fig. 6A). NF-160 and S-100β proteins were expressed in all the groups, confirming the formation of myelin sheaths composed of SCs and the ingrowth of new axons in the 4D-printed gel and fCNT-gel. The highest NF-160 expression was observed in the sham group containing intact nerve fibers. Notably, the expression of NF-160 was higher in the fCNT-gel conduits than in the gel conduits (Fig. 6(A and B)). For S-100β, the sham group showed the least expression due to the absence of any regeneration, whereas the gel and fCNT-gel conduits exhibited increased S-100β expression due to neo-tissue formation (Fig. 6(A and C)). Notably, the fCNT-gel exhibited higher expression of S-100β when compared to the gel-NGC group. Thus, the conductive fCNT fillers augmented the efficacy of the 4D-printed gel conduit.

Histology of the vital organs, including the brain, spleen, kidneys, and liver, in gel and fCNT-gel implanted NGC groups revealed minimal inflammation in response to the implanted materials (Fig. S6†). These observations further underscore the superior biocompatibility of the 4D-printed NGCs.

There are few reports on 3D-printed multifunctional conductive hydrogels for applications in diverse areas.[50] In this study, nanofillers of high electrical conductivity, namely, CNTs, were functionalized with carboxylic acid groups to improve their dispersion and interaction with the hydrogel matrix of alginate and methylcellulose. The composite gel (fCNT-gel) exhibited excellent electrical conductivity and mechanical stability and exhibited good sensing capabilities while detecting human movements, such as elbow and finger

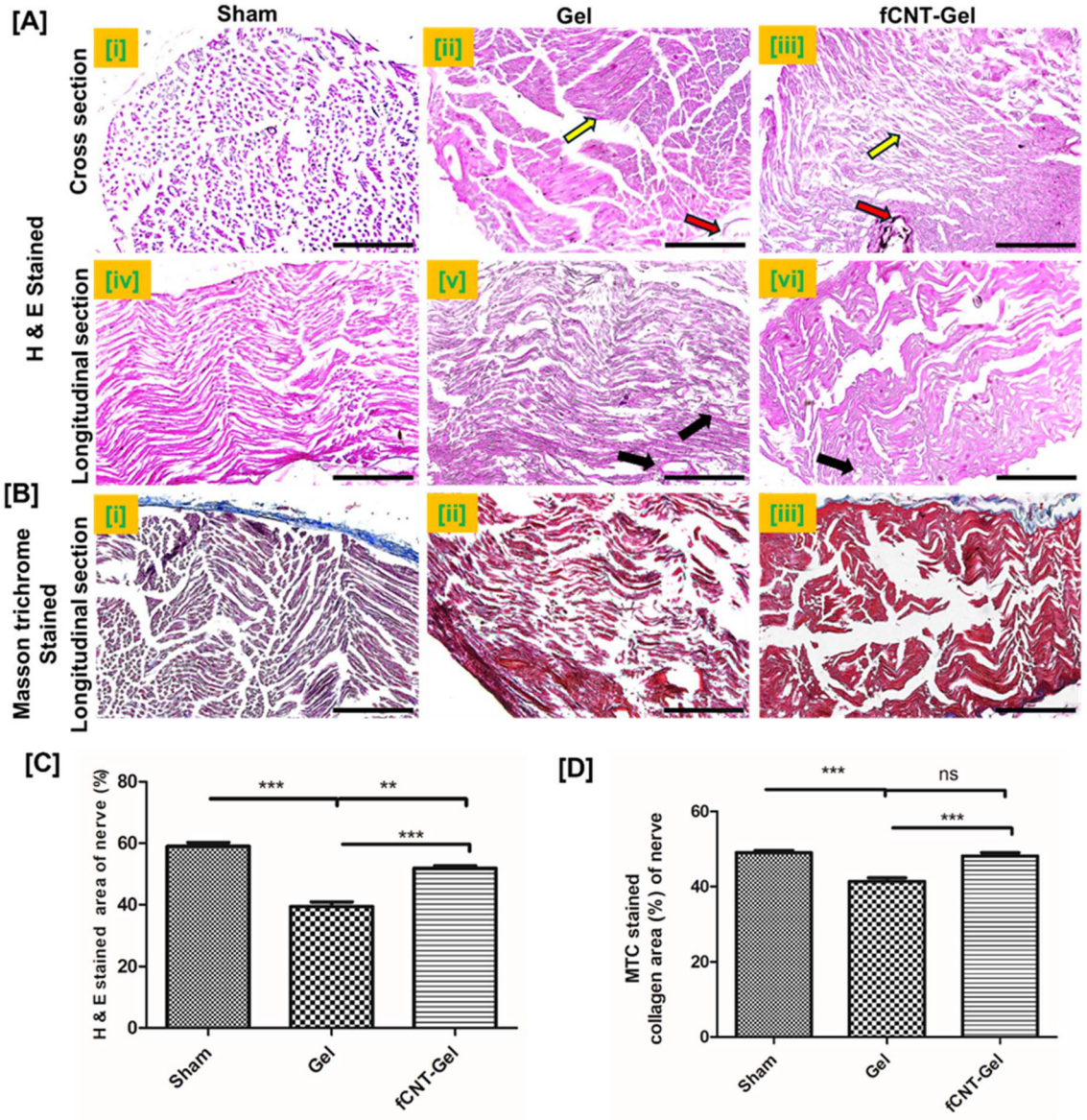

Fig. 5 Assessment of the nerve regeneration potential of 4D-printed conduits (gel and fCNT-gel) through histological analysis. (A) Bright-field images of H&E-stained transverse and longitudinal slices of sciatic nerves of rats belonging to various groups: (i and iv) Sham, (ii and v) gel, and (iii and vi) fCNT-gel groups (scale: 200 μm) (the yellow arrow indicates regenerated nerve fibers, the red arrow identifies the remnants of the scaffold, and the black arrow signifies the blood vessel within the regenerated nerve fibers); (B) bright-field images of Mason trichrome-stained longitudinal slices of sciatic nerves of rats belonging to (i) sham, (ii) gel, and (iii) fCNT-gel groups; (C) and (D) quantification of (C) H&E-stained and (D) Masson's trichrome-stained positive area. Data are presented as mean ± SD (n = 4).

bending. Conductive hydrogels used for strain sensing are usually stretchable, with some of them exhibiting tensile strain as high as ≈140%. The conductivity varies from 0.018 mS cm^{-1} to 180 mS cm^{-1}, depending on whether it is ionic or electronic conductivity, the kind of nanofiller, interaction with the polymer matrix, *etc*. However, they lack multifunctional attributes, such as printability, self-folding features, and biocompatibility. While the fCNT-gel prepared in this study had a tensile strain of ≈15%, it was sufficient to sense subtle human motions, such as finger bending. Moreover, it retained its printability and self-folding ability due to significant swelling differences between the layers. Most conductive gels for NGCs are limited to simple designs[27] and require complex chemistries to synthesize.[51] NGCs with self-wrapping abilities have been demonstrated in a few studies by using chitosan films with an encapsulated cryogel[52] and a bi-layered gel of poly(*N*-isopropylacrylamide) (PNIPAm) and alginate.[53] Currently, there are no reports of NGCs that can integrate electrical cues with self-folding ability, which can give rise to new avenues in designing next-generation NGCs with superior neural regeneration capabilities. In this study, complex designs of NGCs were prepared, including multichannel and bifurcated, which

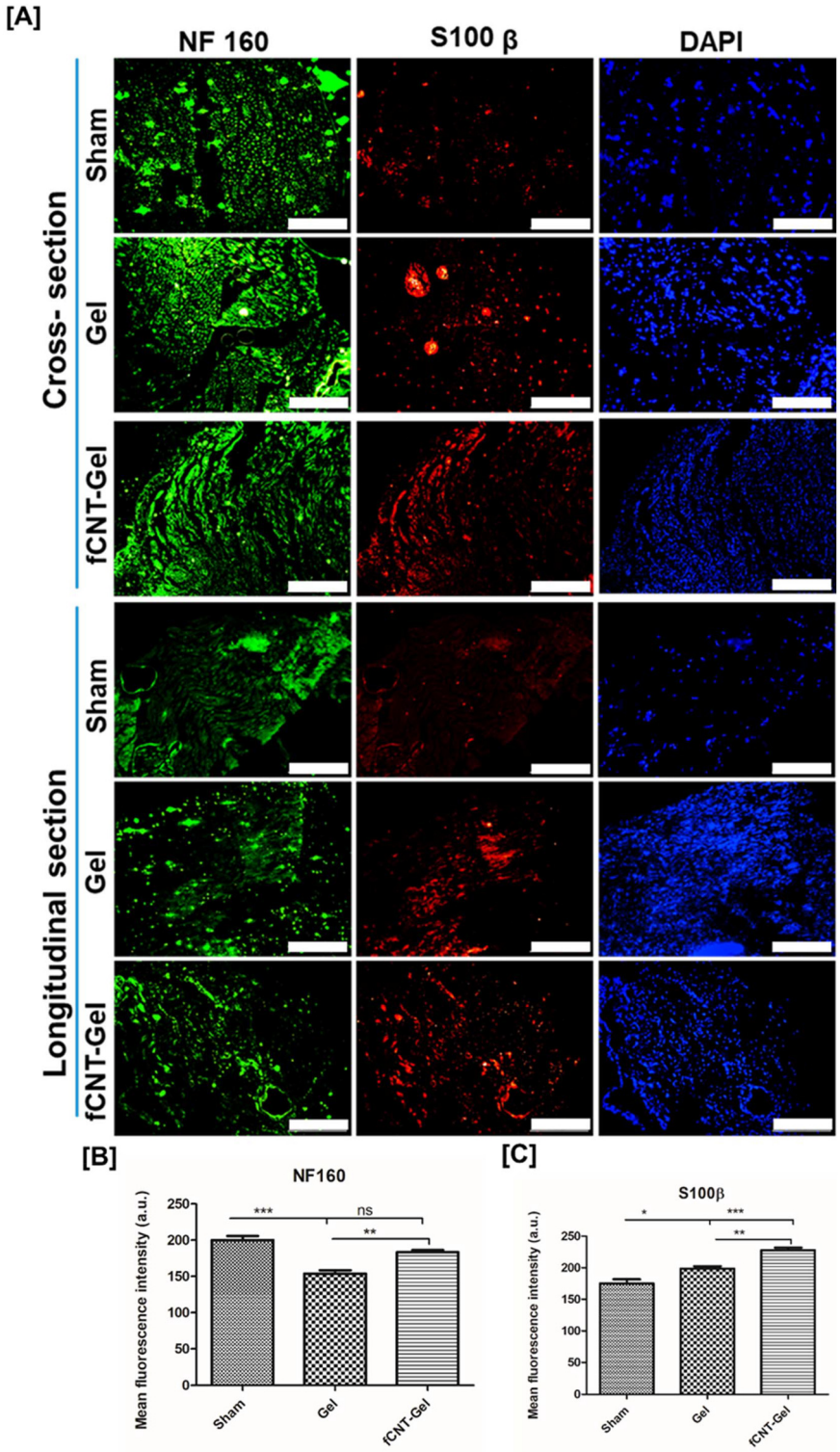

Fig. 6 Assessment of the nerve regeneration potential of 4D-printed conduits through histology. (A) Cross-sectional and longitudinal sections of sciatic nerves stained for NF-160 (green) (a marker for neurofilaments), S-100β (red) (Schwann cell marker), and nuclei (blue) (scale (cross-sections): 100 μm, scale (longitudinal sections): 200 μm); (B and C) Plots of fluorescence intensity for (B) NF-160 and (C) S-100β (* and ** denote $p < 0.05$ and $p < 0.01$, respectively). Data are presented as mean ± SD ($n = 4$).

would be highly useful in regenerating large nerve defects in thicker fascicular nerves. While the current multi-channel NGCs have diameters (in the range of 5–6 mm) larger than that of the sciatic nerve of rodent models, further optimization can enhance the extent of bending in the printed structures to achieve smaller diameter multi-channel NGCs suitable for *in vivo* implantation. Additionally, the fCNT-gels exhibited superior neural regeneration potential compared to sham and gel groups in sciatic nerve defects of rats.

3. Conclusion

This study demonstrates the potential of multifunctional conductive hydrogels prepared by additive manufacturing for diverse applications. fCNT-gels exhibited excellent electrical conductivities (6.6 ± 0.5 mS cm^{-1}) and mechanical properties. They were employed as flexible strain sensors to detect subtle human motions, such as elbow and finger bending, with excellent reproducibility and accuracy. Physiologically mimetic and complex NGC designs, such as multichannel and bifurcated, were prepared using design-aided additive manufacturing. fCNT-gels were also endowed with non-invasive imaging capabilities, such as X-ray imaging. fCNT-gels exhibited higher cell proliferation and adhesion *in vitro* compared to neat gels. The synergistic effect of electrical cues and the *in situ* self-folding ability of hydrogels enabled sutureless neurorrhaphy and superior neural regeneration. fCNT-gels led to excellent *in vivo* peripheral nerve regeneration in rat models when compared to neat gels and sham groups. The 4D-printed conductive hydrogels can open newer avenues to develop next-generation NGCs and other applications, such as strain sensors.

Conflicts of interest

The authors have filed a patent application. No other conflicts to declare.

Data availability

Data will be made available on request.

Acknowledgements

The authors greatly acknowledge the Anusandhan National Research Foundation (ANRF), Government of India (IPA/2020/000025). A. J. was supported by the IoE Postdoctoral Fellowship of the Indian Institute of Science. S. C. was supported by the Prime Minister's Research Fellowship. The authors thank Prof. G. K. Ananthasuresh for the technical inputs on the FEA simulations performed in the study.

References

1 S. Oh, S. Lee, S. W. Kim, C. Y. Kim, E. Y. Jeong, J. Lee, D. A. Kwon and J.-W. Jeong, *Biosens. Bioelectron.*, 2024, **258**, 116328.
2 F. Geng, Y. Li, Q. Wu and C. Ding, *Sens. Actuators, B*, 2025, **422**, 136625.
3 Z. Wang, H. Bai, W. Yu, Z. Gao, W. Chen, Z. Yang, C. Zhu, Y. Huang, F. Lv and S. Wang, *Sci. Adv.*, 2022, **8**, eabo1458.
4 Y. Ohm, C. Pan, M. J. Ford, X. Huang, J. Liao and C. Majidi, *Nat. Electron.*, 2021, **4**, 185–192.
5 Y. Wang, P. Zhu, M. Tan, M. Niu, S. Liang and Y. Mao, *Adv. Intell. Syst.*, 2023, **5**, 2300162.
6 L. Wang, Z. Lou, K. Jiang and G. Shen, *Adv. Intell. Syst.*, 2019, **1**, 1900040.
7 L. Yan, S. Liu, J. Wang, X. Ding, Y. Zhao, N. Gao, Z. Xia, M. Li, Q. Wei, O. V. Okoro, Y. Sun, L. Nie, A. Shavandi, G. Jiang, J. Chen, L. Fan and Y. Weng, *Adv. Funct. Mater.*, 2024, **34**, 2402698.
8 F. Zhu, J. Lin, Z. L. Wu, S. Qu, J. Yin, J. Qian and Q. Zheng, *ACS Appl. Mater. Interfaces*, 2018, **10**, 13685–13692.
9 C. Cai, H. Zhu, Y. Chen, C. Chen, H. Li, Z. Yang and H. Liu, *Appl. Mater. Today*, 2022, **27**, 101491.
10 Y. Liang, X. Zhao, T. Hu, B. Chen, Z. Yin, P. X. Ma and B. Guo, *Small*, 2019, **15**, 1900046.
11 L. Wang, Y. Wu, T. Hu, P. X. Ma and B. Guo, *Acta Biomater.*, 2019, **96**, 175–187.
12 J. Liu, W. Wang, H. Li, P. Huo, P. Teng, H. Ding and X. Shen, *Eur. Polym. J.*, 2024, **208**, 112895.
13 X. Chen, C. Liu, Z. Huang, X. Pu, L. Shang, G. Yin and C. Xue, *J. Biomed. Mater. Res., Part A*, 2019, **107**, 2784–2795.
14 S. Das, M. Sharma, D. Saharia, K. K. Sarma, E. M. Muir and U. Bora, *Biomed. Mater.*, 2017, **12**, 045025.
15 A. Magaz, B. F. Spencer, J. G. Hardy, X. Li, J. E. Gough and J. J. Blaker, *ACS Biomater. Sci. Eng.*, 2020, **6**, 6906–6916.
16 R. Jaswal, S. Shrestha, B. K. Shrestha, D. Kumar, C. H. Park and C. S. Kim, *Mater. Sci. Eng., C*, 2020, **116**, 111213.
17 J. Wang, L. Tian, N. Chen, S. Ramakrishna and X. Mo, *Mater. Sci. Eng., C*, 2018, **91**, 715–726.
18 X. Fang, H. Guo, W. Zhang, H. Fang, Q. Li, S. Bai and P. Zhang, *J. Mater. Chem. B*, 2020, **8**, 10593–10601.
19 L.-Y. Hsiao, L. Jing, K. Li, H. Yang, Y. Li and P.-Y. Chen, *Carbon*, 2020, **161**, 784–793.
20 C. Wu, A. Liu, S. Chen, X. Zhang, L. Chen, Y. Zhu, Z. Xiao, J. Sun, H. Luo and H. Fan, *ACS Appl. Mater. Interfaces*, 2019, **11**, 22152–22163.
21 S. He, J. Wu, S.-H. Li, L. Wang, Y. Sun, J. Xie, D. Ramnath, R. D. Weisel, T. M. Yau and H.-W. Sung, *Biomaterials*, 2020, **258**, 120285.
22 Y. Xu, P. A. Patsis, S. Hauser, D. Voigt, R. Rothe, M. Günther, M. Cui, X. Yang, R. Wieduwild and K. Eckert, *Adv. Sci.*, 2019, **6**, 1802077.
23 P. Madhusudanan, G. Raju and S. Shankarappa, *J. R. Soc., Interface*, 2020, **17**, 20190505.
24 M. Rahman, T. Mahady Dip, R. Padhye and S. Houshyar, *J. Biomed. Mater. Res., Part A*, 2023, **111**, 1916–1950.

25 H. Samadian, H. Maleki, A. Fathollahi, M. Salehi, S. Gholizadeh, H. Derakhshankhah, Z. Allahyari and M. Jaymand, *Int. J. Biol. Macromol.*, 2020, **154**, 795–817.
26 C. Gao, S. Song, Y. Lv, J. Huang and Z. Zhang, *Macromol. Biosci.*, 2022, **22**, 2200051.
27 J. Park, J. Jeon, B. Kim, M. S. Lee, S. Park, J. Lim, J. Yi, H. Lee, H. S. Yang and J. Y. Lee, *Adv. Funct. Mater.*, 2020, **30**, 2003759.
28 W. Jing, Q. Ao, L. Wang, Z. Huang, Q. Cai, G. Chen, X. Yang and W. Zhong, *Chem. Eng. J.*, 2018, **345**, 566–577.
29 Z.-F. Zhou, F. Zhang, J.-G. Wang, Q.-C. Chen, W.-Z. Yang, N. He, Y.-Y. Jiang, F. Chen and J.-J. Liu, *ACS Biomater. Sci. Eng.*, 2016, **2**, 1572–1581.
30 S. Choudhury, A. Joshi, V. S. Baghel, G. K. Ananthasuresh, S. Asthana, S. Homer-Vanniasinkam and K. Chatterjee, *J. Mater. Chem. B*, 2024, **12**, 5678–5689.
31 S. Choudhury, A. Joshi, D. Dasgupta, A. Ghosh, S. Asthana and K. Chatterjee, *Mater. Adv.*, 2024, **5**, 3345–3356.
32 S. H. Kim, Y. B. Seo, Y. K. Yeon, Y. J. Lee, H. S. Park, M. T. Sultan, J. M. Lee, J. S. Lee, O. J. Lee, H. Hong, H. Lee, O. Ajiteru, Y. J. Suh, S.-H. Song, K.-H. Lee and C. H. Park, *Biomaterials*, 2020, **260**, 120281.
33 S. Li, H. Yang, G. Chen, J. Zheng, W. Wang, J. Ren, C. Zhu, Y. Yang, Y. Cong and J. Fu, *Chem. Eng. J.*, 2023, **473**, 145444.
34 V. Vannaladsaysy, S. Choudhury, S. Datta and K. Chatterjee, *Smart Mater. Struct.*, 2025, **34**, 055004.
35 A. Joshi, S. Choudhury, S. Asthana, S. Homer-Vanniasinkam, U. Nambiar and K. Chatterjee, *Biomater. Sci.*, 2023, **11**, 7703–7708.
36 Z. Wang, Y. Zheng, L. Qiao, Y. Ma, H. Zeng, J. Liang, Q. Ye, K. Shen, B. Liu, L. Sun and Z. Fan, *Adv. Healthcare Mater.*, 2024, **13**, 2401093.
37 A. Joshi, S. Choudhury, V. S. Baghel, S. Ghosh, S. Gupta, D. Lahiri, G. Ananthasuresh and K. Chatterjee, *Adv. Healthcare Mater.*, 2023, **12**, 2300701.
38 T. Ebbesen, H. Lezec, H. Hiura, J. Bennett, H. Ghaemi and T. Thio, *Nature*, 1996, **382**, 54–56.
39 L. Lavagna, R. Nisticò, S. Musso and M. Pavese, *Mater. Today Chem.*, 2021, **20**, 100477.
40 G. Li, C. Li, G. Li, D. Yu, Z. Song, H. Wang, X. Liu, H. Liu and W. Liu, *Small*, 2022, **18**, 2101518.
41 X. Sun, Z. Qin, L. Ye, H. Zhang, Q. Yu, X. Wu, J. Li and F. Yao, *Chem. Eng. J.*, 2020, **382**, 122832.
42 I. I. Stoyanova, R. J. A. van Wezel and W. L. C. Rutten, *J. Neural Eng*, 2013, **10**, 066018.
43 L. Yao, G. C. W. de Ruiter, H. Wang, A. M. Knight, R. J. Spinner, M. J. Yaszemski, A. J. Windebank and A. Pandit, *Biomaterials*, 2010, **31**, 5789–5797.
44 J. Wang, H. Xiong, T. Zhu, Y. Liu, H. Pan, C. Fan, X. Zhao and W. W. Lu, *ACS Nano*, 2020, **14**, 12579–12595.
45 C. R. Carvalho, J. M. Oliveira and R. L. Reis, *Front. Bioeng. Biotechnol.*, 2019, **7**, 337.
46 S. Datta, S. Jana, A. Das, A. Chakraborty, A. R. Chowdhury and P. Datta, *Bioact. Mater.*, 2020, **5**, 569–576.
47 S. Ghosh, S. Haldar, S. Gupta, A. Bisht, S. Chauhan, V. Kumar, P. Roy and D. Lahiri, *ACS Appl. Bio Mater.*, 2020, **3**, 5796–5812.
48 P. Gupta, A. Agrawal, K. Murali, R. Varshney, S. Beniwal, S. Manhas, P. Roy and D. Lahiri, *Mater. Sci. Eng., C*, 2019, **97**, 539–551.
49 K. Matsumoto, C. Sato, Y. Naka, R. Whitby and N. Shimizu, *Nanotechnology*, 2010, **21**, 115101.
50 J. Liu, J. Garcia, L. M. Leahy, R. Song, D. Mullarkey, B. Fei, A. Dervan, I. V. Shvets, P. Stamenov, W. Wang, F. J. O'Brien, J. N. Coleman and V. Nicolosi, *Adv. Funct. Mater.*, 2023, **33**, 2214196.
51 Z. Yi, F. Zhan, Y. Chen, R. Zhang, H. Lin and L. Zhao, *Chem. Eng. J.*, 2023, **478**, 147261.
52 T. B. Aigner, C. Haynl, S. Salehi, A. O'Connor and T. Scheibel, *Mater. Today Bio*, 2020, **5**, 100042.
53 J. Xiao, Z. Yu, Y. Tian, M. Zeng, B. Su, J. Ding, C. Wu, D. Wei, J. Sun and H. Fan, *Sens. Actuators, B*, 2024, **413**, 135917.